

Bound spinons in an antiferromagnetic $S=\frac{1}{2}$ chain with a staggered field

M. Kenzelmann^{1,2}, Y. Chen^{1,3}, C. Broholm^{1,2}, D. H. Reich,¹ and Y. Qiu^{2,4}

(1) *Department of Physics and Astronomy, Johns Hopkins University, Baltimore, Maryland 21218*

(2) *NIST Center for Neutron Research, National Institute of Standards and Technology, Gaithersburg, Maryland 20899*

(3) *Los Alamos National Laboratory, Los Alamos, NM 87545*

(4) *Department of Materials Science and Engineering, University of Maryland, College Park, Maryland, 20742.*

(Dated: November 11, 2018)

Inelastic neutron scattering was used to measure the magnetic field dependence of spin excitations in the antiferromagnetic $S=\frac{1}{2}$ chain $\text{CuCl}_2 \cdot 2(\text{dimethylsulfoxide})$ (CDC) in the presence of uniform and staggered fields. Dispersive bound states emerge from a zero-field two-spinon continuum with different finite energy minima at wave numbers $q=\pi$ and $q_i \approx \pi(1 - 2\langle S_z \rangle)$. The ratios of the field dependent excitation energies are in excellent agreement with predictions for breather and soliton solutions to the quantum sine-Gordon model, the proposed low-energy theory for $S=\frac{1}{2}$ chains in a staggered field. The data are also consistent with the predicted soliton and $n=1,2$ breather polarizations and scattering cross sections.

PACS numbers: 75.25.+z, 75.10.Jm, 75.40.Gb

Shortly after the advent of quantum mechanics, Hans Bethe introduced a model antiferromagnet that continues to play a central role in quantum many body physics [1]. The isotropic antiferromagnetic (AF) spin-1/2 chain, has a simple spin Hamiltonian: $\mathcal{H} = J \sum_n \mathbf{S}_n \cdot \mathbf{S}_{n+1}$, is integrable through Bethe's Ansatz, and is realized with high fidelity in a number of magnetically anisotropic Cu^{2+} based materials. Because it sits at the boundary between quantum order and spin order at $T = 0$, Bethe's model is ideally suited for exploring quantum critical phenomena and the qualitatively different phases that border the critical point [2, 3]. This letter presents an experimental study of the profound effects of a symmetry breaking staggered field on excitations in the spin-1/2 chain.

In zero field, the fundamental excitations of the spin-1/2 chain are not spin waves but domain wall like quasi-particles called spinons that separate reversed AF domains [4, 5, 6]. The ground state is a Luttinger liquid and the spinons are non-local spin-1/2 objects with short range interactions. Thus, spinons can only be excited in pairs and produce a gapless continuum. Such a spectrum has been observed in several quasi-one-dimensional spin-1/2 chain systems [7, 8, 9] and is now understood to be a distinguishing attribute of quantum-critical systems. The dramatic effect of a staggered field was discovered through a high field neutron scattering experiment on the quasi-one-dimensional spin-1/2 antiferromagnet copper benzoate [10]. Designed to verify theoretical predictions of a field driven gapless incommensurate mode [5], this experiment instead revealed a field induced gap in the excitation spectrum. The critical exponent of $\sim 2/3$ describing the field dependence of the gap in copper benzoate, $[\text{PMCu}(\text{NO}_3)_2 \cdot (\text{H}_2\text{O})_2]_n$ [11], and Yb_4As_3 [12], identified the source of this gap as the staggered field that accompanies a uniform field in materials with alternating Cu-coordination. The staggered field yields an energetic distinction between reversed domains, which

confines spinons in multi-particle bound states [13].

A quantitative theory for this effect was developed by Affleck and Oshikawa starting from the following extension of Bethe's model Hamiltonian [13, 14],

$$\mathcal{H} = J \sum_i \mathbf{S}_i \mathbf{S}_{i+1} + \sum_j (-1)^j \mathbf{D} \cdot (\mathbf{S}_{j-1} \times \mathbf{S}_j) - \sum_{j,\alpha,\beta} H^\alpha [g_{\alpha\beta}^u + (-1)^j g_{\alpha\beta}^s] S_j^\beta. \quad (1)$$

The alternating spin environment is represented by the staggered Dzyaloshinskii-Moriya (DM) interaction and Zeeman terms. Through an alternating coordinate transformation, the model can be mapped to a spin-1/2 chain in a transverse staggered field that is proportional to the uniform field H . While the zero field properties of Eq.(1) are indistinguishable from Bethe's model, an applied field induces transverse AF Ising spin order and a gap. Using bosonization techniques to represent the low energy spin degrees of freedom, Affleck and Oshikawa showed that their dynamics is governed by the quantum sine-Gordon model (QSG) with Lagrangian density

$$\mathcal{L} = \frac{1}{2} [(\partial_t \bar{\phi})^2 - (\partial_x \bar{\phi})^2] + hC \cos(\beta \bar{\phi}). \quad (2)$$

Here $h \propto H$ is the effective staggered field. $C(H)$ and $\beta(H)$ (which goes to $\sqrt{2\pi}$ for $H \rightarrow 0$) vary smoothly with the applied field and can be determined numerically through the Bethe Ansatz for $h \ll H$ [14, 15].

With applications from classical to particle physics, the SG model plays an important role in the theory of non-linear dynamic systems [16]. Excitations are composed of topological objects called solitons that encompass a localized $\pm 2\pi/\beta$ shift in $\bar{\phi}$ for a soliton and anti-soliton respectively [17]. In addition there are soliton-antisoliton bound states called breathers, which drop below the soliton-anti-soliton continuum as the non-linear

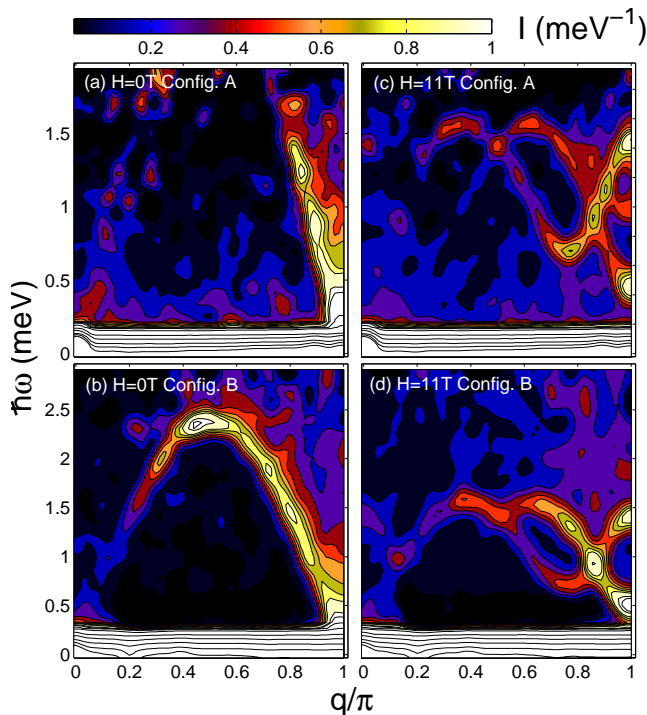


FIG. 1: Normalized scattering intensity $I(q, \omega)$ in zero field and $H=11$ T in the $S=\frac{1}{2}$ chain CDC as a function of the chain wave-vector transfer q and energy transfer $\hbar\omega$, measured at $T=40$ mK. The data were binned and smoothed, leading to an effective wave-vector resolution $\delta q=0.057\pi$ and 0.061π and an energy resolution 0.1 and 0.18 meV for configurations A and B, respectively. The colorbar indicates the scattering strength.

term is increased. The excited state wave functions are known for both solitons and breathers, which enables exact calculation of the inelastic scattering cross sections. In this Letter we use neutron scattering from a magnetized spin-1/2 chain with two spins per unit cell to test these results and more generally to explore the dynamics of spinons with long range interactions.

Based on the temperature dependence of the susceptibility and specific heat, $\text{CuCl}_2 \cdot 2((\text{CD}_3)_2\text{SO})$ (CDC) was identified as an AF $S=\frac{1}{2}$ chain system with $J=1.5$ meV, a staggered g -tensor and/or DM interactions [18, 19]. The spin chains run along the \mathbf{a} -axis of the orthorhombic crystal structure ($Pnma$) [20], with the Cu^{2+} ions separated by $0.5\mathbf{a} \pm 0.22\mathbf{c}$. Wave vector transfer is indexed in the corresponding reciprocal lattice $\mathbf{Q}(hkl) = h\mathbf{a}^* + k\mathbf{b}^* + l\mathbf{c}^*$, and we define $q = \mathbf{Q} \cdot \mathbf{a}$. Due to weak inter-chain interactions, CDC has long-range AF order in zero field below $T_N=0.93$ K with an AF wave-vector $\mathbf{Q}_m = \mathbf{a}^*$. An applied field strongly suppresses the ordered phase [19], indicating that inter-chain interactions favor correlations that are incompatible with the field-induced staggered magnetization[21]. Above the $H_c = 3.9$ T critical field for Néel order, we find that CDC is an excellent model system for our purpose.

Deuterated single crystals were grown through slow cooling of saturated methanol solutions of anhydrous copper chloride and deuterated dimethyl sulfoxide ($(\text{CD}_3)_2\text{SO}$) in a 1:2 molar ratio [19]. The sample studied consisted of four crystals with a total mass 7.76 g. The experiments were performed using the disk chopper time-of-flight spectrometer (DCS) at the NIST Center for Neutron Research with the \mathbf{c} -axis and the magnetic field vertical. In configuration A the incident energy was $E_i=3.03$ meV and the \mathbf{a} -axis was parallel to the incident neutron beam direction \mathbf{k}_i . Configuration B had $E_i=4.64$ meV and $\angle(\mathbf{k}_i, \mathbf{a})=60^\circ$. The counting time was 18 hrs at 11 T and an average of 5 hrs for each measurement between 0 and 8T. The raw scattering data were corrected for a time-independent background measured at negative energy transfer, for monitor efficiency, and for the Cu^{2+} magnetic form factor, folded into the first Brillouin zone, and put onto an absolute scale using the elastic incoherent scattering from CDC. For the normalization, the H/D ratio ($=0.02$) was measured independently through prompt- γ neutron activation analysis.

Figures 1(a) and 1(b) show that for $T \ll J/k_B$, the zero-field excitation spectrum of CDC consists of continuum scattering above a low-energy threshold that varies as $\hbar\omega = \frac{\pi}{2}J|\sin(q)|$ through the zone [5]. An exact analytical expression for the two spinon contribution to the scattering cross section which accounts for 72.89% of the total spectral weight was recently obtained by Bougourzi *et al.* [6, 22, 23]. Figures 2 and 3 show a quantitative comparison of this result (blue line), duly convoluted with the experimental resolution, to the experimental data. The excellent quantitative agreement between model and data provides compelling evidence for spinons in the zero field state of CDC. Note that the Goldstone modes that are expected due to Néel order for $\hbar\omega < k_B T_N \approx 0.1$ meV, are not resolved in this experiment.

Figures 1(c) and 1(d) show that the magnetic excitations in CDC change dramatically with field and are dominated by resolution-limited modes for $H = 11$ T. Figures 2 and 3(b) show spectra at the wave vectors corresponding to the minima in the dispersion relations, which occur at $q = \pi$, and $q_i = 0.77\pi$, as determined from the constant- $\hbar\omega$ cut in Fig. 3(a). These data graphically illustrate the field-induced transfer of spectral weight from the two-spinon continuum into single-particle excitations. A phenomenological cross-section of long-lived dispersive excitations was fit to the data near $q = \pi$ and q_i to take into account the experimental resolution and thereby accurately locate the excitation energies. These fits are shown as red lines in Figs. 2 and 3, and the inferred parameters characterizing the dispersion relations are displayed for a series of fields in Fig. 4.

We now examine whether our high field observations are consistent with the QSG model for spin-1/2 chains in a staggered field [14]. First, the model predicts single soliton excitations at $q_i = \pi(1 - 2\langle S_z \rangle)$. This is qualita-

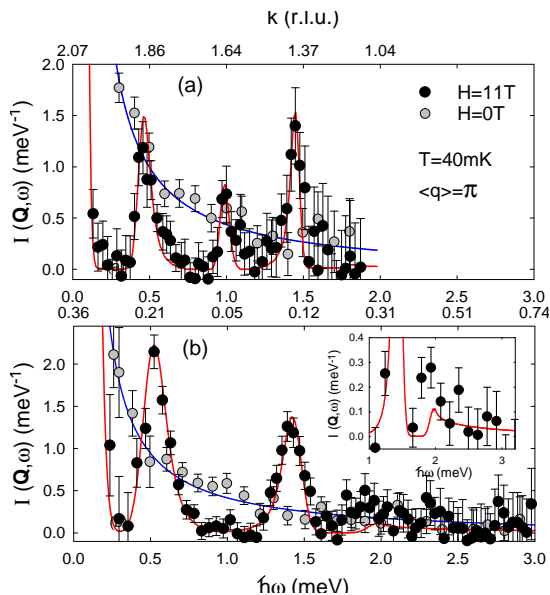


FIG. 2: Spectra at $q=\pi$ observed with configurations A (a) and B (b) for zero field and 11 T obtained from data in the range $0.95\pi < q < 1.05\pi$. The zero-field intensity for $0.3\pi < q < 0.4\pi$ was subtracted as a background. The top axes indicate wave-vector transfer, k , perpendicular to the chain. The blue line is a fit of the two-spinon cross-section to the zero field scattering [6]. The red lines are fits to the $H = 11$ T data as explained in the text, including the theoretically calculated breather continua polarized perpendicular to the field [15]. The inset in (b) highlights the high energy range.

tively consistent with the raw data in Figs. 1(c) and 1(d), and with Fig. 4(d), which shows how q_i moves across the zone with H . Quantitative agreement is also apparent from the solid line in Figure 4(d), which is the predicted field dependence as calculated from the magnetization curve for a spin-1/2 chain [5].

The soliton and antisoliton mass is related to the exchange interaction of the original spin chain and the uniform and staggered fields, H and h , as follows [14, 17]

$$M \approx J \left(\frac{g\mu_B h}{J} \right)^{(1+\xi)/2} \times \left\{ B \left(\frac{J}{g\mu_B H} \right)^{(2\pi-\beta^2)/4\pi} \left(2 - \frac{\beta^2}{\pi} \right)^{1/4} \right\}^{-(1+\xi)/2}. \quad (3)$$

Here $\xi = \beta^2/(8\pi - \beta^2) \rightarrow 1/3$ for $H \rightarrow 0$ and $B = 0.422169$. Assuming $h \propto H$, the soliton energy versus field is shown as a solid red line in Fig. 4(a). While Eq. (3) is at the limit of validity for CDC at $H = 11$ T, we attribute the discrepancy with the mode energy at q_i (red triangles) to inter-chain interactions that suppress the effective staggered field close to H_c . The more general expression, $h \propto (H - H_c)^\alpha$, yields a good fit for $\alpha = 0.68(5)$ (dashed red line).

The QSG model predicts that breather bound states of $2n$ -solitons should be accessible at $q=\pi$ with masses

$$M_n = 2M \sin(n\pi\xi/2). \quad (4)$$

Sharp modes are indeed observed in CDC at $q = \pi$. Their

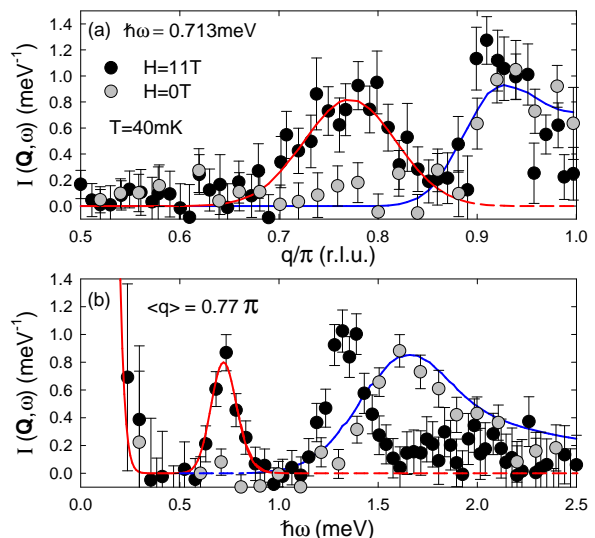


FIG. 3: Constant- ω (a) and constant- q scans (b) through the gapped soliton at $H=11$ T at the incommensurate wave-vector q_i . The zero-field scattering is shown for comparison together with a fit of the two-spinon cross-section to the data. The unfitted peak corresponds to a moving breather. These data are from configuration B. The ranges of integration were (a) $0.675 \text{ meV} < \hbar\omega < 0.75 \text{ meV}$, and (b) $0.72\pi < q < 0.82\pi$.

energies are compared to the breather masses predicted for $h \propto H$ (solid lines) and $h \propto (H - H_c)^{0.68}$ (dashed lines) in Fig. 4(a). The ratios of the commensurate and putative breather mode energies to the lowest energy incommensurate and putative soliton mode energy, shown in Fig. 4(b), are in excellent agreement with the normalized breather energies M_n/M for $n=1$ and $n=2$. This comparison, which is insensitive to the origin of the staggered field, suggests that breathers indeed exist in CDC.

The evidence for breathers is strengthened as we examine the polarization of the scattering at $q = \pi$. According to the QSG model, n -odd (even) breathers are polarized in the plane normal to \mathbf{H} and perpendicular (parallel) to \mathbf{h} [15]. Neutron scattering probes the projection of spin fluctuations on the plane normal to the scattering vector \mathbf{Q} . Figure 2 shows that the $\hbar\omega=1$ meV peak seen for $\mathbf{Q}_A \approx (1, 1.64, 0)$ in configuration A is absent for $\hbar\omega=1$ meV and $\mathbf{Q}_B \approx (1, 0, 0)$ in configuration B. In a quasi-one-dimensional system the only explanation for this is that the excitation is polarized along $\mathbf{Q}_B \parallel \mathbf{a} \parallel \mathbf{h}$ as expected for an even numbered breather, and hence is extinguished by the polarization factor in the neutron scattering cross section for configuration B. The predicted \mathbf{b} and \mathbf{c} axis polarizations respectively of the $n=1$ breather and the soliton are confirmed by the consistent polarization factor corrected intensities from configurations A and B for $H = 11$ T in Fig. 4(c).

One of the unusual aspects of the QSG model is that complex features such as the breather and soliton structure factors can be calculated exactly [15]. The solid

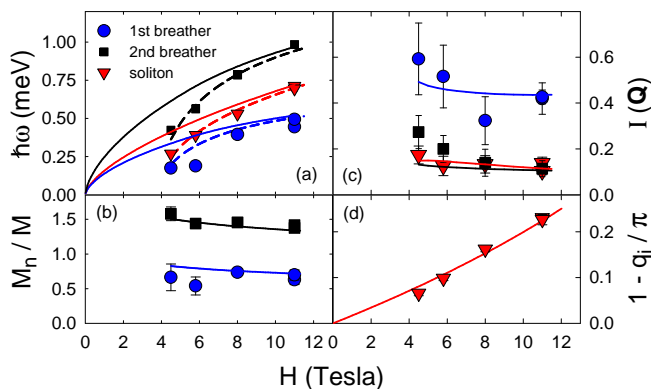


FIG. 4: (a) Field dependence of the soliton and breather modes. The lines are the QSG predictions for $h \propto H$ (solid) and $h=c(H-H_c)^{0.68}$ (dashed). (b) Ratio of breather energies to soliton energies versus H , compared to the QSG model. (c) Energy integrated intensities divided by the QSG predicted polarization factors and compared to structure factor predictions using particle energies given by the dashed line in (a) and a common overall scale factor [15]. (d) Incommensuration q_i obtained from the minimum in the soliton dispersion compared to the predicted $q_i = \pi(1 - 2\langle S_z \rangle)$ using the magnetization curve $\langle S_z \rangle = 1/\pi \arcsin((1 - \pi/2 + \pi J/(g_z H \mu_B))^{-1})$ for a Heisenberg spin-1/2 chain[5]. The field dependence was measured with configuration A, and an additional measurement at $H = 11$ T was performed using configuration B.

lines in Fig. 4(c) show that these exact results are consistent with the field dependent intensities of the commensurate and incommensurate low energy modes in CDC. For $H = 11$ T the third breather is expected at about 1.4 meV, close to the energy of the soliton mode at $h=1$. The peak close to 1.4 meV has intensity $I = 0.14(3)$ in configuration A and $I = 0.26(2)$ in configuration B and this is consistent with a third breather contribution polarized along **b**. The inferred **b**-polarized intensity of $I_b^{\text{exp}} = 0.23(7)$ is however much greater than the intensity predicted for the $n = 3$ breather ($I_3^{\text{QSG}} = 0.026(7)$), which indicates additional anisotropic contributions to the inelastic scattering there.

In addition to the field-induced resonant modes, the experiment shows that a high energy continuum persists for $H=11$ T. Fig. 1(d) for example clearly shows a broad maximum in the q -dependence of neutron scattering for energies $\hbar\omega > 1.6$ meV and $q \approx \pi$. Firm evidence for continuum scattering comes from the field dependence of the first moment $\langle \hbar\omega \rangle_{\mathbf{Q}} = \hbar^2 \int S(\mathbf{Q}, \omega) \omega d\omega$, which is proportional to the ground state energy $\langle \mathcal{H} \rangle$ with a negative q -dependent prefactor [24]. At zero field the experimental value of $\langle \hbar\omega \rangle_{\mathbf{Q}}$ corresponds to $\langle \mathcal{H} \rangle = -0.4(1)J$, in agreement with Bethe's result of $\langle \mathcal{H} \rangle = (\frac{1}{4} - \ln 2)J \approx -0.44J$. At 11 T, however, $\langle \tilde{\mathcal{H}} \rangle$ derived solely from the resonant modes is $-0.25(6)J$ when $\langle \mathcal{H} \rangle$ is expected to be $-0.34J$ [19]. The discrepancy is an independent indication of spectral weight beyond the resonant modes. For $q = \pi$, the transverse contribution to the continuum scattering

predicted by the QSG model [15] and shown as a solid line in the inset of Fig. 2 has a maximum close to a weak peak in the measured scattering intensity. The shortfall of the theoretical result suggests that there are additional longitudinal contributions to the continuum scattering.

In summary, staggered field induced spinon binding in spin-1/2 chains provides an experimental window on the unique non-linear dynamics of the quantum sine-Gordon model. Our neutron scattering experiment on quasi-one-dimensional CDC in a high magnetic field yields clear evidence for soliton/antisoliton creation at wave vector transfer $q = \pi(1 - 2\langle S_z \rangle)$, as well as $n = 1$ and $n = 2$ breather bound states at $q = \pi$. Interpretation of the data throughout the Brillouin zone will require exact diagonalization studies and a better understanding of lattice effects than provided by the continuum field theory reviewed in this paper. Other results that call for further experimental and theoretical work are the observation of high energy continuum scattering in the gapped phase and indications that inter-chain interactions can renormalize the soliton mass.

We thank C. P. Landee, J. Copley, C. Batista, I. Affleck, and F. Essler for helpful discussions and R. Paul for prompt gamma analysis. Work at JHU was supported by the NSF through DMR-0306940. DCS and the high-field magnet at NIST were supported in part by the NSF through DMR-0086210 and DMR-9704257.

-
- [1] H. Bethe, Z. Phys. **71**, 205 (1931).
 - [2] S. Sachdev, *Quantum Phase Transitions*, Cambridge University Press (2000).
 - [3] C. Broholm, *et al.*, in *High Magnetic Fields: Applications in condensed matter physics and spectroscopy*, C. Berthier *et al.*, Eds. Springer Verlag (2002).
 - [4] L. D. Faddeev *et al.*, Phys. Lett. A **85**, 375 (1981).
 - [5] G. Müller *et al.*, Phys. Rev. B **24**, 1429 (1981).
 - [6] M. Karbach *et al.*, Phys. Rev. B **55**, 12510 (1997).
 - [7] D. A. Tennant *et al.*, Phys. Rev. B **52**, 13368 (1995).
 - [8] D. Dender *et al.*, Phys. Rev. B **53**, 2583 (1996).
 - [9] M. B. Stone *et al.*, Phys. Rev. Lett. **91**, 037205 (2003).
 - [10] D. C. Dender *et al.*, Phys. Rev. Lett. **79**, 1750 (1997).
 - [11] R. Feyerherm *et al.*, J. Phys. Cond. Mat. **12**, 8495 (2000).
 - [12] M. Kohgi *et al.*, Phys. Rev. Lett. **86**, 2439 (2001).
 - [13] M. Oshikawa *et al.*, Phys. Rev. Lett. **79**, 2883 (1997).
 - [14] I. Affleck *et al.*, Phys. Rev. B **60**, 1038 (1999).
 - [15] F. H. L. Essler *et al.*, Phys. Rev. B **57**, 10592 (1998) and *ibid* **68**, 064410 (2003).
 - [16] A. M. Tsvelik, *Quantum Field Theory in Condensed Matter Physics*, Cambridge University Press (1995).
 - [17] R. F. Dashen *et al.*, Phys. Rev. D **11**, 3424 (1975).
 - [18] C. P. Landee *et al.*, Phys. Rev. B **35**, 228 (1987).
 - [19] Y. Chen and *et al.*, unpublished.
 - [20] R. D. Willett *et al.*, Inorg. Chem. Acta **4**, 447 (1970).
 - [21] M. Sato and M. Oshikawa, Phys. Rev. B in press (2004).
 - [22] A. H. Bougourzi *et al.*, Phys. Rev. B **54**, R12669 (1996).
 - [23] A. Fledderjohann *et al.*, Phys. Rev. B **53**, 11543 (1996).
 - [24] P. C. Hohenberg *et al.*, Phys. Rev. B **10**, 128 (1974).